

# Silicon nanocrystals-based electroluminescent resistive switching device <sup>EP</sup>

Cite as: J. Appl. Phys. **126**, 144501 (2019); <https://doi.org/10.1063/1.5119299>

Submitted: 10 July 2019 . Accepted: 15 September 2019 . Published Online: 08 October 2019

J. L. Frieiro <sup>id</sup>, J. López-Vidrier <sup>id</sup>, O. Blázquez <sup>id</sup>, D. Yazıcıoğlu, S. Gutsch, J. Valenta <sup>id</sup>, S. Hernández <sup>id</sup>, M. Zacharias <sup>id</sup>, and B. Garrido <sup>id</sup>

## COLLECTIONS

<sup>EP</sup> This paper was selected as an Editor's Pick



View Online



Export Citation



CrossMark

## ARTICLES YOU MAY BE INTERESTED IN

[On the origin of the enhancement of defect related visible emission in annealed ZnO micropods](#)

Journal of Applied Physics **126**, 145104 (2019); <https://doi.org/10.1063/1.5111184>

[Hybrid plasmonic metasurfaces](#)

Journal of Applied Physics **126**, 140901 (2019); <https://doi.org/10.1063/1.5116885>

[Simultaneous determination of thermal diffusivity and thermal conductivity of a thin layer using double modulated thermal excitations](#)

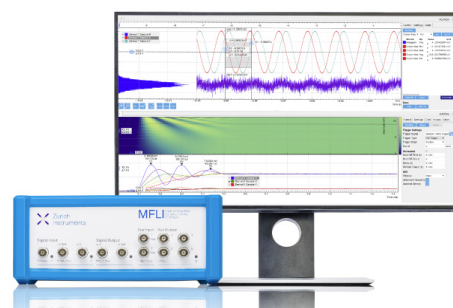
Journal of Applied Physics **126**, 145103 (2019); <https://doi.org/10.1063/1.5116526>

## Challenge us.

What are your needs for periodic signal detection?



Zurich  
Instruments



# Silicon nanocrystals-based electroluminescent resistive switching device

Cite as: J. Appl. Phys. **126**, 144501 (2019); doi: [10.1063/1.5119299](https://doi.org/10.1063/1.5119299)

Submitted: 10 July 2019 · Accepted: 15 September 2019 ·

Published Online: 8 October 2019







View Online



Export Citation



CrossMark

J. L. Frieiro,<sup>1,2,a)</sup>  J. López-Vidrier,<sup>3,b)</sup>  O. Blázquez,<sup>1,2</sup>  D. Yazicioğlu,<sup>3</sup>  S. Gutsch,<sup>3</sup>  J. Valenta,<sup>4</sup>   
S. Hernández,<sup>1,2</sup>  M. Zacharias,<sup>3</sup>  and B. Garrido<sup>1,2</sup> 

## AFFILIATIONS

<sup>1</sup>MIND, Departament d'Enginyeria Electrònica i Biomèdica, Universitat de Barcelona, Martí i Franquès 1, 08028 Barcelona, Spain

<sup>2</sup>Institute of Nanoscience and Nanotechnology (IN<sup>2</sup>UB), Universitat de Barcelona, Av. Diagonal 645, 08028 Barcelona, Spain

<sup>3</sup>Laboratory of Nanotechnology, IMTEK, Faculty of Engineering, Albert-Ludwigs Universität Freiburg, Georges-Köhler-Allee 103, 79110 Freiburg, Germany

<sup>4</sup>Faculty of Mathematics and Physics, Charles University, Ke Karlovu 3, 121 16 Prague 2, Czech Republic

<sup>a)</sup>[jfrieiro@el.ub.edu](mailto:jfrieiro@el.ub.edu)

<sup>b)</sup>[julia.lopez.vidrier@imtek.uni-freiburg.de](mailto:julia.lopez.vidrier@imtek.uni-freiburg.de)

## ABSTRACT

In the last few years, the emergence of studies concerning the resistive switching (RS) phenomenon has resulted in the finding of a large amount of materials being capable of acting as an active layer in such devices, i.e., the layer where the change in resistance takes place. Whereas the normal operation consists of the electrical readout of the modified resistance state of the device after electrical writing, electro-photonic approaches seek the involvement of light in these devices, be it either for the active Set or Reset operations or the readout. We propose in this work silicon nanocrystal multilayers (Si NC MLs) as an active material for being used in RS devices, taking advantage of their outstanding optical properties. The resistance states of Si NC MLs were obtained by electrical excitation, whose readout is carried out by electrical and electro-optical means, thanks to a distinguishable electroluminescence emission under each state. To achieve this, we report on an adequate design that combines both the Si NC MLs with ZnO as a transparent conductive oxide, whose material properties ensure the device RS performance while allowing the electro-optical characterization. Overall, such an occurrence states the demonstration of a Si NCs-based electroluminescent RS device, which paves the way for their future integration into photonic integrated circuits.

© 2019 Author(s). All article content, except where otherwise noted, is licensed under a Creative Commons Attribution (CC BY) license (<http://creativecommons.org/licenses/by/4.0/>). <https://doi.org/10.1063/1.5119299>

## I. INTRODUCTION

Although the resistive switching (RS) phenomenon had been known for many years, it was in 2008 when the first fully operational RS device was realized.<sup>1</sup> Materials presenting the RS phenomenon, typically dielectrics, exhibit inner structural modification after an electric field is applied through the two sandwiching electrodes, resulting in controlled changes in resistivity under certain electrical polarities.<sup>2</sup> This novel property allows dielectric materials to act, when embedded in the proper device structure, as resistive random-access memory (RRAM) devices that operate between at least two well-defined states, thus performing as digital memories.<sup>3</sup> Indeed, the occurrence of RS between two well-defined resistance states is widely accepted to be caused by the formation of a conductive

filament (CF) across the dielectric material which, according to the most established models, takes place via either the atomic diffusion from the metallic electrodes toward the dielectric (electrochemical metallization, ECM)<sup>4</sup> or the generation of oxygen vacancies due to oxygen atom diffusion from the oxide-based dielectric toward the electrodes (valence change mechanism, VCM).<sup>5,6</sup> The cyclic generation and destruction of the CF has been investigated in a wealth of dielectric and semiconductor materials, aiming not only at the full understanding of the fundamental properties of the RS phenomenon but also at the determination of the optimum conditions for long-lasting performance (that is, improved properties of a RRAM device).<sup>7,8</sup> Heterogeneous materials such as Si suboxides are of high interest, since they are compatible with current electronic technologies. Within

this context, previous works have been led by the group of Kenyon by employing a TiN/SiO<sub>x</sub>/TiN structure devoted to understanding the role of the dielectric/electrode interfaces in the CF formation and destruction processes,<sup>9,10</sup> and to demonstrate that the presence of Si nanoinclusions might as well contribute to the switching operation of the dielectric layer.<sup>11</sup>

The improved electronic properties yielded by nanostructured silicon in comparison to its bulk counterpart have led, during the last few decades, to the in-depth investigation of their underlying fundamentals, in order to optimize their performance to be applied in the electronics and optoelectronics fields. In particular, the quantum confinement effect, that is, the spatial confinement of the carrier wavefunctions within the nanostructure, induces the relaxation of the band-to-band transition selection rules as well as an increase of the Si bandgap energy that can be controlled by decreasing the particle size.<sup>12,13</sup> Within the whole range of Si nanostructures, matrix-embedded Si nanocrystals have provided, thanks to their versatility and robustness, a model platform for examining the structural, optical, and electrical properties of semiconductors at the nanoscale level. Several works have been published that pursued the determination of the physical mechanisms governing the optical<sup>14–16</sup> and electrical<sup>17–19</sup> performance of SiO<sub>2</sub>-embedded Si NCs, aiming at their applications as an active emitting layer in light-emitting diode (LED) structures.<sup>20–22</sup> Indeed, it is the size-dependence of the Si NC properties what makes this material system of great interest and, consequently, the adequate control of NCs size and shape has focused much effort. Within this context, arranging the NCs along multilayers (MLs) has led to excellent control by depositing nanometer-thin Si-rich oxide (SiO<sub>x</sub>) layers between stoichiometric SiO<sub>2</sub> barriers, the latter efficiently limiting the Si excess diffusion from the SiO<sub>x</sub> layers during the postdeposition high-temperature annealing. The final process induces the precipitation and crystallization of the Si excess into ordered arrays of Si NC superlattices.<sup>23,24</sup>

Recently, new attempts on semiconductor and electronics industries to be adapted to the needs of the field of photonics, aiming at fast light-based and material-free interconnections, constitute the development of the novel concept of “optical memristor” as a requisite for the future in RRAM industry. The ability to optically write or read (or both) the resistance state in a RS memory will increase the overall device operation speed and provide a direct signal conversion, while making this new technology fully-compatible with the photonic integrated circuits (PICs). Although not fully exploited, some reports on the optical memristor field exist. Mehonic *et al.* published on the effect of light writing of SiO<sub>x</sub>-based RRAM devices, the generated photoconductivity inducing permanent state switching until light incidence was stopped, thus demonstrating the possibility of achieving light-triggered resistance switching.<sup>25</sup> Furthermore, the group of Leuthold has worked on optically-read electrically-written memristors within a waveguide (WG) structure, where surface plasmon polariton generation at the interface between amorphous Si and the active WG material (Si) led to different optical losses (and thus different readout) of the light beam through the WG.<sup>26</sup> Another functionality which has not yet been fully explored is electroluminescence (EL), i.e., an active optical response to electrical stimuli in each resistance state after electrical writing. This occurrence has the advantage of having the electrical and optical source integrated

within the same device,<sup>27</sup> instead of requiring external laser sources for writing (light-triggered RRAM devices)<sup>25</sup> or reading (through WG structure).<sup>26,28,29</sup> Recent studies have reported on structures containing Si NCs/SiO<sub>2</sub> MLs as an active memristive layer, where not only the RS properties of Si NC MLs were inspected but also the role played by the number of Si NC/SiO<sub>2</sub> bilayers on the CF formation was addressed.<sup>30</sup> Given these demonstrations and their well-known EL properties, Si NC MLs become a great active layer candidate to develop “electroluminescent memristors.” Electroluminescence in Si NCs, be it governed by either bipolar carrier injection<sup>31,32</sup> or impact excitation,<sup>33,34</sup> can be strongly influenced by the formation of a CF through the nanostructures, which, in turn, may serve as a distinguishable signature between both resistance states. It is this different EL emission at each resistance state which can be exploited in PICs as an indicator of the device memory state, and its modulation paves the way to novel integrated optical RS devices for photonic applications.

In this work, we demonstrate ZnO/Si NCs-based devices as electroluminescent RRAM devices. For this, we embedded Si NC MLs as the dielectric material (I) into a metal-insulator-semiconductor (MIS) device design, where intrinsically *n*-type ZnO (M) serves as a top transparent conductive oxide (TCO), and *p*-type Si is employed as the substrate (S). Herein, we show that not only EL emission can be achieved in a controlled way from this MIS device system but also Si NCs provide a characteristic EL signal that allows distinguishing the resistance state of the device, desirable for optical resistance switching applications.

## II. EXPERIMENTAL DETAILS

Devices consisting of a MIS structure have been fabricated using Si NCs/SiO<sub>2</sub> MLs on top of a Si substrate, with a ZnO electrode as top transparent contact,<sup>35</sup> as sketched in Fig. 1(a). Plasma-enhanced chemical vapor deposition (PECVD) was the selected technique to deposit five Si-rich oxynitride (SRON)/SiO<sub>2</sub> bilayers on top of a *p*-type Si substrate, with nominal layer thicknesses of 4.5 nm and 1 nm, respectively, following the superlattice approach.<sup>24</sup> The stoichiometry of the SRON layer was held constant at SiO<sub>0.93</sub>N<sub>0.23</sub>, which corresponds to a Si excess of [Si]<sub>exc</sub> = 17 at. %. An additional 2-nm-thin Si<sub>3</sub>N<sub>4</sub> sublayer was inserted between the substrate and the first SRON sublayer, which was found to promote electron injection in inversion conditions due to the contained fixed positive charges as a consequence of its defective nature.<sup>35,36</sup> The ML samples underwent an annealing treatment at 1150 °C for 1 h under N<sub>2</sub> ambient in a quartz tube furnace, to promote the precipitation and crystallization of the Si excess within the SRON layers in the form of Si NCs. The material fabrication process was completed by passivating the samples with H<sub>2</sub> at 450 °C, in order to get rid of undesired dangling bonds. For more details on the ML deposition, the reader is kindly directed to Ref. 37.

A direct observation of the sample structure was done via energy-filtered transmission electron microscopy (EFTEM), using a JEOL 2010F instrument (field emission gun operating at 200 keV). To perform EFTEM, the instrument was equipped with a Gatan Image Filter (with a resolution of 0.8 eV), which

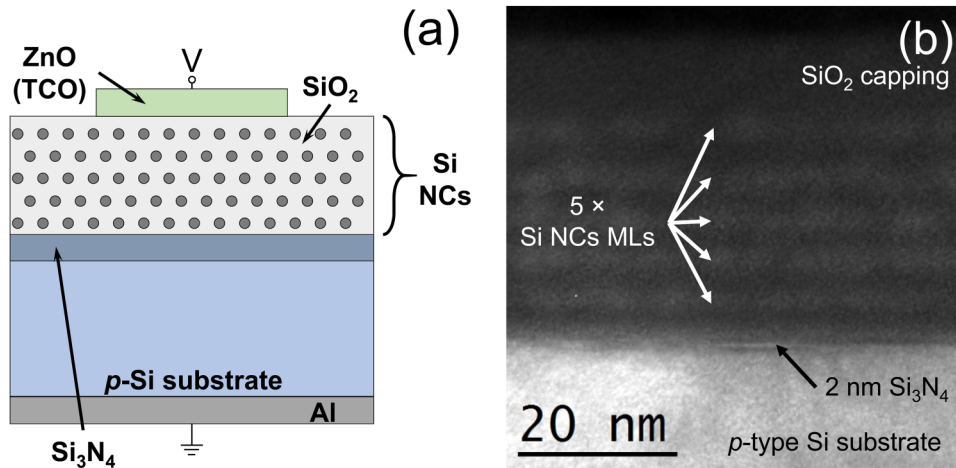


**FIG. 1.** (a) Sketch of the MIS device structure containing the Si NC MLs as the insulator (I) layer, and ZnO (*n*-type TCO) and Si substrate (*p*-type) as metal (M) and semiconductor (S) layers, respectively. For the electrical and electro-optical characterization, voltage was applied at the top electrode while the bottom was grounded. Thicknesses are not to scale. (b) EFTEM image of an equally-deposited sample, where the Si NCs can be identified in the ML structure, deposited over a Si substrate and with a capping of SiO<sub>2</sub> (which was later removed for device processing).

allowed filtering the signal around the Si plasmon energy ( $E_{Si} \sim 17$  eV). Prior to the TEM inspection, the samples were prepared by mechanical flat polishing and final low angle Ar<sup>+</sup>-ion milling. As it can be observed in Fig. 1(b), the real thickness of the final structure, measured by EFTEM, is in good agreement with the nominal thickness of  $\sim 30$  nm. The image also confirms that the Si NCs layers are clearly separated in the pristine state of the sample, with no percolation through them whatsoever (previous studies have shown that percolation appears for silicon excess above  $[Si]_{exc} = 38\text{--}44$  at. %<sup>38,39</sup>).

Aiming at the electroluminescence performance of the devices, ZnO (intrinsically *n*-type) was employed as top TCO (resistivity of  $0.1 \Omega \text{ cm}$  and  $\sim 75\%$  transparency throughout the whole visible spectrum),<sup>40,41</sup> which was deposited on top of the MLs by means of atomic layer deposition (ALD) and afterwards photolithography-patterned to achieve  $500\text{-}\mu\text{m}$ -diameter circular contacts (total device area of  $\sim 2 \times 10^{-3} \text{ cm}^2$ ). Finally, for the back contact, the Si substrate was full-area Al metallized via evaporation. Further details on the preparation of analogous devices can be found elsewhere.<sup>35,37</sup>

For the electrical characterization, the devices were loaded into a Cascade Microtech Summit 11000 probe station, properly screened from external electromagnetic noise by means of a Faraday cage. The current-voltage [ $I(V)$ ] characteristics were performed using an Agilent B1500 semiconductor device analyzer. Finally, EL spectra were acquired via a Princeton Instruments LN<sub>2</sub>-cooled CCD coupled to a monochromator (400–1100 nm range).

### III. RESULTS

#### A. RS cycle characterization

To attain knowledge on the RS behavior of Si NC MLs, the devices were submitted to full  $I(V)$  cycles, the voltage being applied at the ZnO top electrode, as shown in Fig. 1(a). In particular, Fig. 2 displays a representative set of ten  $I(V)$  cycles out of one of the several device structures measured, using 50 mV steps. Indeed, the curves exhibit easily-identifiable bipolar resistive

switching characteristics, which are described as follows: (1) a first sweep to positive voltages ( $V > 0$ ) on the pristine device structure (red curve) results in monotonous current increase until  $V = 9.5$  V, (2) at which a sudden increase in current takes place. This process is known as “electroforming,” and it is typically ascribed to the first formation of CFs through the dielectric layer.<sup>5</sup> Anticipating the electroforming process, we set the current compliance (CC) at  $100 \mu\text{A}$ , which was found to be the most adequate one to allow the CF formation while avoiding permanent damage to the device. This electroforming process was found to be very stable in all the measured devices, always occurring at a voltage of

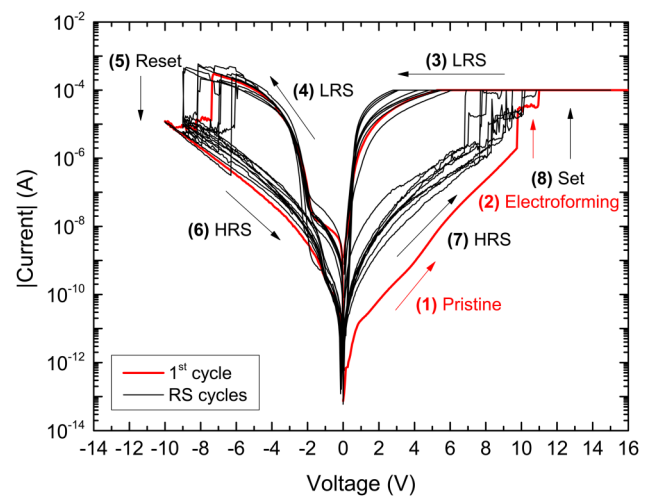


**FIG. 2.** Typical current (in absolute value) vs voltage curves of the Si NC ML structure under study, showing controlled bipolar RS cycles. In red, the first cycle, corresponding to the pristine state, the electroforming process ( $\sim 10$  V) and the first Reset of the device; in black, the following  $I(V)$  curves until completing 10 RS cycles. Current compliance of  $100 \mu\text{A}$  was employed for  $V > 0$ .

$10 \pm 0.5$  V. (3) The backwards voltage sweep down to  $V = 0$  V shows a very high conductivity in comparison to the pristine state, due to the inner structural modification within the MLs: the device lays now within the low resistance state (LRS). (4) Voltage is then increased toward negative polarity ( $V < 0$ ), exhibiting again low resistivity. Two different conduction regimes can be observed in LRS, while the device is under substrate accumulation conditions. The first regime, down to  $-2$  V, is due to the current displacement of the trapped charge in the structure, basically in defects present either in the ZnO electrode or in the active Si NCs MLs; in the second regime, beyond  $-2$  V, electron injection from the top electrode already dominates conduction. When  $-8$  V are reached, the current suddenly drops by almost two orders of magnitude. (5) This is called the “Reset” process, and it is attributed in the literature to the partial destruction of the CF.<sup>2,42</sup> Afterwards, the device lays within the high resistance state (HRS). (6) Again, the backwards voltage sweep down to  $V = 0$  V induces no modification of the resistive state of the device. (7) Last, following a positive voltage sweep, (8) the switch from HRS to LRS can be achieved through the recovery of the CF due to their reduction in the Set process, induced in our device beyond  $V = 8$  V. Note that the HRS is more conductive than the pristine state (hence the term “partial” is used for the destruction of the CF in the Reset process).<sup>5</sup>

Overall, the various RS cycles recorded showed Set and Reset voltage values spanning from 7 V to 10 V and from  $-6$  V to  $-9$  V, respectively, which states a nearly symmetric performance with a relatively low dispersion. This, added to the 2 orders of magnitude in the current difference between LRS and HRS at a read voltage of  $V_{\text{read}} = -4$  V (where conduction mechanisms are well established in both resistance states), makes this device structure a good candidate for controlled RS cycling,<sup>3</sup> where future improvements can be developed to reduce the voltage ranges of operation and the requirement of a CC. Finally, it must also be mentioned that, after multiple cycles, we have detected an increasing current level for the HRS both in negative and positive polarization, which can be related to the low overall endurance of the analyzed devices. No other trends have been observed neither in the LRS current levels nor in the Set and Reset voltages. Therefore, this occurrence indicates that the failure of the devices, always taking place in the form of an almost permanent LRS, could be attributed to the formation of CFs with lower reoxidation state after every new cycle.

## B. Electroluminescence emission

The well-known EL properties of SiO<sub>2</sub>-embedded Si NCs make this material an adequate research platform to study the effect of the RS phenomenon on the light emission properties of the structure under study. In order to simultaneously characterize both properties that the active layer exhibits, device structures were submitted to the electroforming process and additional RS cycles following the process previously described in Sec. III A. The characterization of the EL emission was then performed by having each device in one of the two stable states (LRS and HRS) and applying a constant voltage while both monitoring the current (to check that the resistance state under study is maintained throughout the

measurement of the emission) and acquiring the emitted EL spectra. The voltage range analyzed was selected to include the Set and Reset processes previously observed in the electrical characterization and employing a voltage step of 1 V, resulting in respective ranges for HRS and LRS of  $-8$  V to 8 V and  $-6$  V to 7 V. It must be mentioned here that no clear dependence was found between the number of cycles applied and emission intensity.

In Figs. 3(a) and 3(b), all the spectra collected for one device in both resistance states (HRS and LRS, respectively) are shown, stating a clear difference in emission between the states and a dependence with the voltage applied. In terms of polarity, the structure shows no relevant emission when in substrate inversion conditions ( $V > 0$ ) in LRS. In any other case, when increasing the voltage applied to the structure, the EL also shows a monotonous increase in intensity. Regarding the wavelength dependence of the EL, each state presents a clearly different spectral line shape, whereas HRS shows a peak-like feature, a broad band appears at high applied voltages in LRS, under substrate accumulation ( $V < 0$ ) regime. This already indicates that EL from the device, strongly dependent on the resistance state, might arise from different luminescent centers. A more in-depth characterization of the resulting luminescence was performed for the EL spectra acquired for each resistance state both in the inversion [Fig. 3(c)] and accumulation [Fig. 3(d)] regimes, being the EL optical output read, respectively, at  $V_{\text{read}} = 7$  V and  $V_{\text{read}} = -6$  V. It is important to note that the EL spectra are reproducible when acquired at the mentioned  $V_{\text{read}}$  during several performed RS cycles and in different devices; this essentially means not only that the EL properties hereby shown do have a real sample-related origin (i.e., not related to artefacts), but also that RS cyclability, i.e., stable process reproducibility (see Fig. 2), is also extended to the EL domain.

As already mentioned above, Fig. 3 evidences distinct EL spectral line shape at different resistance states and applied polarities. On the one hand, the inversion regime exhibits, as it can be seen in Fig. 3(c), a clear EL emission, centered around 900 nm, only when the device is in the HRS. This emission is ascribed to radiative recombination of quantum-confined excitons within the Si NCs, as it is well established in the literature and has been previously published by some of the authors.<sup>33–35,43</sup> The emission band is asymmetric, exhibiting a shoulder at shorter wavelengths (higher energies), which can be ascribed to the excitation of several NC size populations. Nevertheless, considering the overall peak position around  $\sim 900$  nm ( $\sim 1.38$  eV), we can estimate a dominant NC mean size of  $\sim 4$  nm, as confirmed by TEM studies and previously reported for equivalent structures.<sup>37,44,45</sup> On the other hand, different EL spectrum line shapes can be found in substrate accumulation conditions, where emission is detected only in the LRS, as observed in Fig. 3(d). The clear broadband emission, from 500 to 1100 nm, resulting in LRS has been deconvolved, in the energy domain, into two Gaussian contributions: a lower energy contribution centered at  $\sim 930$  nm ( $\sim 1.33$  eV, red dotted line) and a broader and higher-energy band around  $\sim 730$  nm ( $\sim 1.70$  eV, magenta dashed line). After immediate comparison to the inversion regime, the lower-energy band can be attributed to quantum-confined emission from the main NC size population; in contrast, the most plausible origin for the higher-energy band is the emission of deep-level radiative defects within the top ZnO electrode, typically

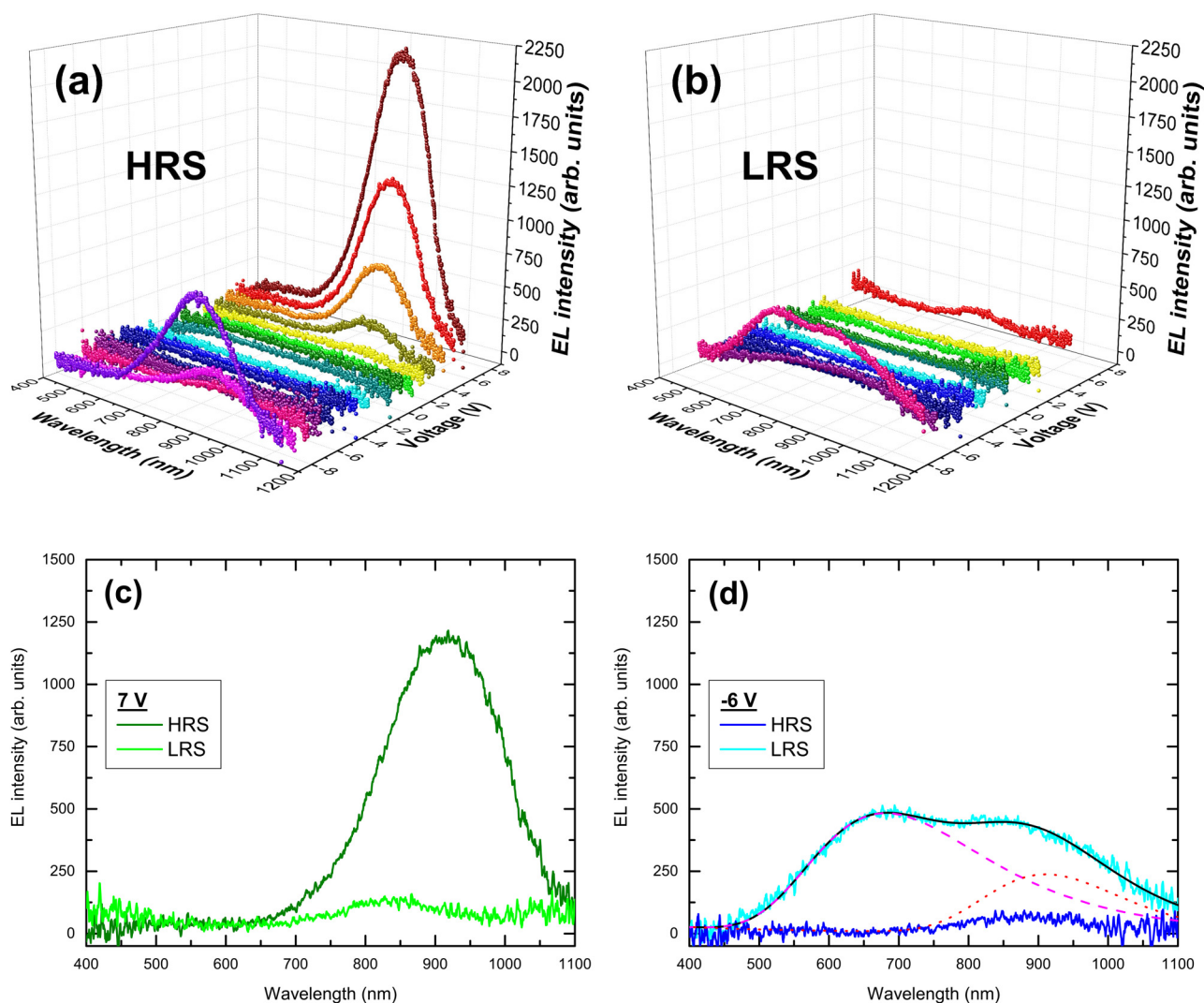


**FIG. 3.** 3-dimensional plots of EL spectra acquired under different  $V_{\text{read}}$ , spanning from  $-8$  V to  $8$  V, corresponding to HRS (a) and LRS (b). The  $V_{\text{read}}$  range was selected from the Set ( $8$  V) to its opposite value passed the Reset ( $-8$  V), in the case of HRS; and from the Reset ( $-6$  V) to the Set ( $7$  V), in the case of LRS. (c) and (d) correspond to the EL spectra yielded by the devices at both HRS and LRS under read conditions: substrate inversion ( $7$  V) and accumulation ( $-6$  V), respectively. For the accumulation regime, deconvolution of the main signal into different-origin contributions is represented with red dotted and magenta dashed lines.

donor-acceptor pairs generated at O vacancies and/or Zn interstitials,<sup>46</sup> as was recently reported in an analogous structure.<sup>43</sup>

From a technological point of view, RS-dependent EL emission means that a controlled direct transduction of the signal output is produced and, therefore, it can be employed for faster and more efficient communication between components in PICs. Therefore, to be employed in this kind of circuits, the signal would have to be detected by a different component of the PIC, which should be able to distinguish between a light-emitting state and a non-emitting one (if using binary logic). In a device structure such as the one we propose here, the operation regime can be described by the integrated EL emission observed in Fig. 4 (obtained after integrating

the EL spectra plotted in Fig. 3), by selecting a reading voltage that yields a large enough difference between the states. By analyzing both polarities in the graph, a good reading voltage may be selected for a maximum difference in emission between states at  $8$  V (inversion regime). Nevertheless, this reading voltage lays well within the Set voltage range, thus implying a conflict in case the device suddenly changes its resistance state. To avoid this, the best voltage value must be kept below (in absolute values) the writing voltage ranges:  $-6$  V to  $-9$  V and  $7$  V to  $10$  V, for Reset and Set operations, respectively. After these considerations, the largest possible EL difference is yielded around  $6$  V, thus making this the best possible reading voltage.

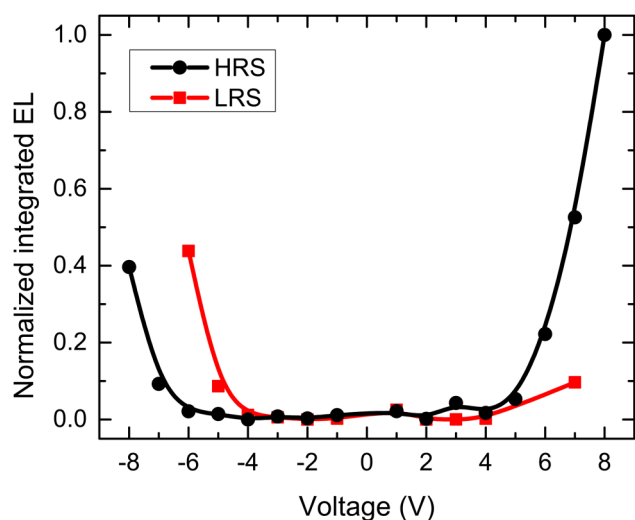


**FIG. 4.** Normalized EL emission intensity obtained by integrating the area under the curve of the spectra plotted in Fig. 3. Both states can be distinguished in accumulation and inversion regimes, but eliminating the Reset and Set voltage ranges, from  $-6$  V to  $-9$  V and from  $7$  V to  $10$  V, respectively; the largest difference between states is found at  $6$  V, making this the optimum reading voltage.

Up to this point we have shown how our ZnO/Si NCs-based RS device structures are capable of giving a distinguishable EL emission in different resistance states when employing reading conditions that have been established for  $6$  V, i.e., not forcing the device to a point where an undesired Set or Reset takes place, while keeping strong EL emission. In particular, quantum-confined Si NCs emission dominates in HRS, although these nanostructures exhibit non-negligible EL even in LRS; instead, a broad band extended to the visible, ascribed to the added emission of ZnO defects, is only observed in LRS. Indeed, the demonstration of such difference in emission between both resistance states makes (*n*) ZnO/Si NC MLs/(*p*)Si MIS structure a good candidate for the novel field of EL memristors.

#### IV. DISCUSSION

The results hereby presented demonstrate a relation between the RS behavior and the EL emission of the (*n*)ZnO/Si NC MLs/(*p*)Si structures under study. Indeed, it is possible to immediately identify the resistance state of the device only by monitoring its emission after electrical excitation at a particular reading voltage value. Four different emissions can be distinguished according to the resistance state and the electrical applied voltage polarity [see Figs. 3(a) and 3(b)], whose main emission features are summarized in Table I. Please note that the different characteristics of the Si NC-related emission poses a clear progress on the optical reading of the resistance state, by yielding a clearly-distinguishable EL emission. In addition, the selection of ZnO as top transparent electrode is far from unintended, and its luminescent centers extended through the visible range ( $>500$  nm) only in

**TABLE I.** Origin of the EL emission from tested structures as observed in Fig. 3, at each resistance state and under different applied voltage polarities.

Resistance state \ voltage polarity	Accumulation ( $V < 0$ )	Inversion ( $V > 0$ )
HRS (CF partially dissolved)	Si NCs (NIR, intense)	Si NCs (NIR, intense)
LRS (CF created)	Si NCs (NIR, weak) ZnO defects (visible)	No EL

LRS and under accumulation regime serve as complementary fingerprint to that of Si NCs.<sup>43</sup>

Going more in depth in this issue, the fact that distinct EL emission is yielded under different resistance states implies that a correlation exists between the structural modification of the layer containing the Si NCs and the electrical excitation of the different luminescent species within the whole system. Therefore, we intend to explain our observations by means of a simple model of the structure under study, as sketched in Fig. 5. With this aim, we will follow the RS cycle as presented in Fig. 2.

As observed by EFTEM [Fig. 1(b)], after the fabrication process, the matrix-embedded Si NCs are arranged along multilayers due to their confined growth through the superlattice approach.<sup>24</sup> This is the so-called pristine state, and it presents periodic SiO<sub>2</sub> barriers between NCs that strongly influence charge transport.<sup>47,48</sup> In this state, positively biasing the top electrode (substrate inversion regime) results in the injection of substrate electrons into the dielectric [Pristine, Fig. 5(a)], giving as a result the emission of Si NCs-related EL. Regarding the possible EL excitation mechanisms, it is still controversial whether bipolar electron-hole injection<sup>31,32</sup> or hot electron impact<sup>34,48</sup> dominate NC excitation within ordered MLs. Under these conditions, being the Si substrate *p*-type, minority carrier (electron) injection from the substrate should be totally quenched, and thus no emission should be observed. Notwithstanding, the thin PECVD-deposited Si<sub>3</sub>N<sub>4</sub> sublayer between substrate and MLs acts as a reservoir of fixed positive charge which, by means of Coulombian attraction, enhances the injection probability of electrons, as recently reported on an analogous device structure.<sup>35</sup> As a result, Si NCs-related emission still takes place; and regarding the excitation mechanisms, hot electron impact is almost certainly the origin of emission, since hole injection from the ZnO electrode can be excluded.

High positive electrical polarity applied at the gate electrode attracts oxygen ions which move toward it, thus generating oxygen vacancies at the Si/SiO<sub>2</sub> interfaces,<sup>49</sup> such as those surrounding Si NCs; therefore, CFs are created through the Si NCs [electroforming, Fig. 5(b)]. The formation of CFs through the NCs is supported by previous observations,<sup>50</sup> and it creates a highly percolated Si NC network along the vertical direction in which carrier confinement is no longer possible. As a consequence, Si NC-related EL emission in LRS in the present electrical polarity is quenched. Please, note that (although it is difficult to confirm without direct observation) the possibility of the CFs being created entirely through the SiO<sub>2</sub> matrix (and not through the NCs) cannot be ruled out. As well, previous works on Si NCs suggest the existence of a SiO<sub>x</sub> shell

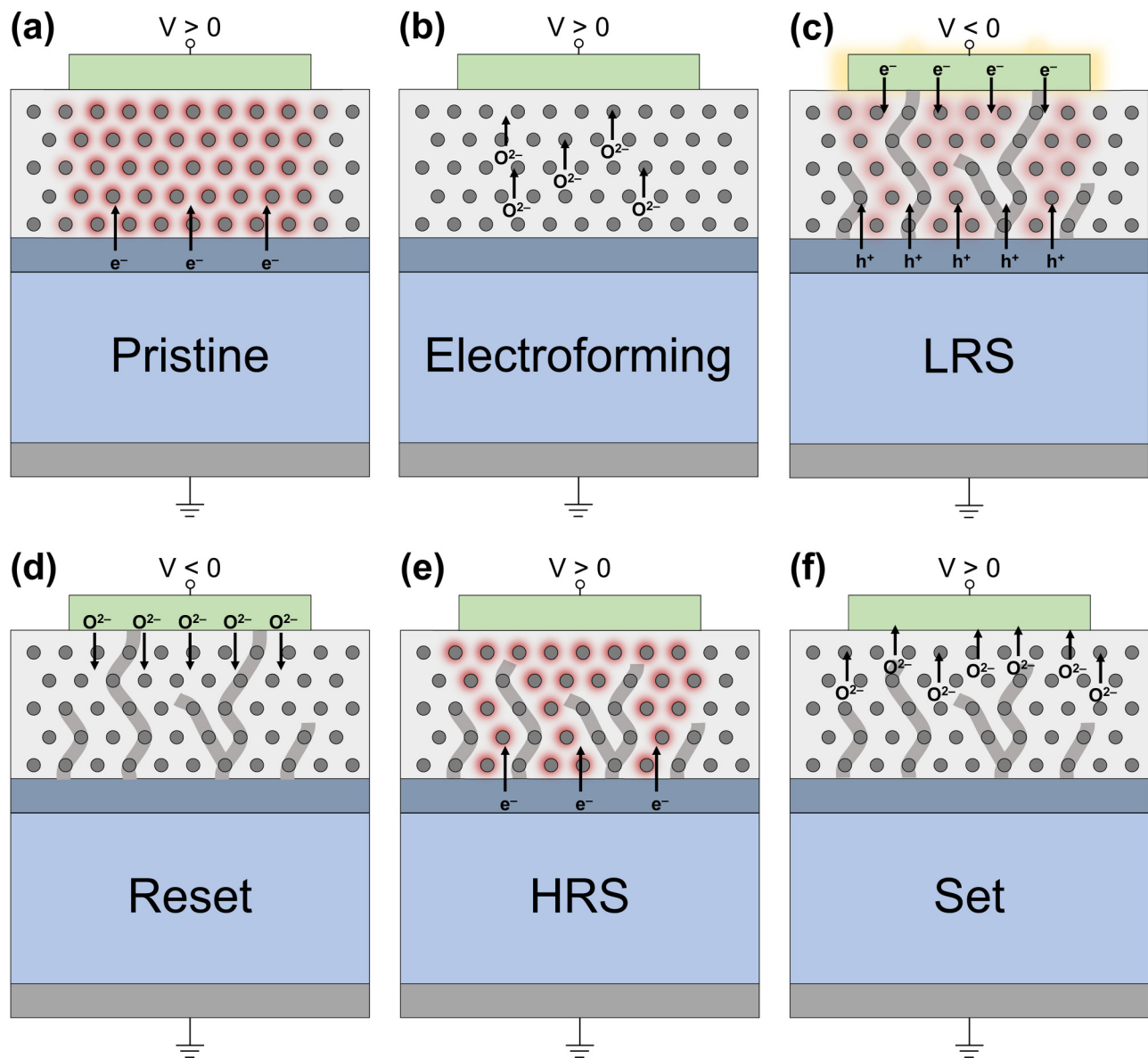


**FIG. 5.** (a) Excitation of the Si NCs in the pristine state. (b) At  $V > 0$ , CF formation takes place within the pristine device (electroforming) through oxygen ion attraction from the MLs toward the ZnO electrode. A nonemitting network of percolating Si NCs is obtained (LRS). (c) At  $V < 0$ , electron-hole pair formation, and thus EL emission, is attained within the Si NCs and the deep-level defect states in ZnO. (d) At high enough negative bias, CF partial reoxidation takes place via oxygen ions diffusing back from the ZnO into the MLs (HRS). Si NC-related EL emission is observed under these conditions. (e) At  $V > 0$ , the  $\text{Si}_3\text{N}_4$  thin layer enhances the minority carrier injection from the substrate, and therefore EL emission from Si NCs is still achieved. (f) Set process, where oxygen ions are again moved toward the ZnO electrode, similar to (a). Arrows indicate charge and ion transport. Luminescent species from which EL is observed, under each resistance state, are shadowed.

surrounding the NC crystalline core,<sup>51</sup> which could generate an additional path for CF formation. In any case, CF formation through oxide cannot modify the description of the phenomena hereby attempted. Regarding the bridging by multiple filaments in contrast to other general explanations that use only one, the model we present is just one possibility that requires of further structural

analysis. The observation of spot-like EL emission distributed along the ZnO electrode (not shown here) supports the assumption of multiple filaments being generated through the active layer, which we will explore in future works. Already in LRS, negative voltage polarity at the top electrode will induce substrate accumulation; under these conditions, electrons are injected from the top



electrode and holes from the Si substrate [Fig. 5(c)]. In spite of conduction through the CF being dominant in this resistance state, conduction along the rest of the device volume may be enough to excite a relevant population of NCs and thus contribute to EL, as experimentally observed [see Fig. 3(d)]. As well, electron-hole pairs can be generated within ZnO deep-levels by either direct electron impact or the injection of holes created at the ZnO/MLs interface, as previously reported.<sup>43</sup> In any case, the final result is the excitation of both luminescent species (Si NCs and ZnO defects) and their consequent EL emission. From a macroscopic point of view, the occurrence of emission coming from the ZnO electrode is supported by the observation of bright visible spots (even with the naked eye) on the surface of the device, which results in electrode damaging due to the high current density reached at the contact points between the CF and the ZnO produced during the Reset process, when current reaches a maximum value circulating through the CF; this damage is still observed after device operation. Through repeated visual inspection of the device, no increase of the damaged areas has been observed after it first takes place during the first cycle.

Under negative bias, and using high enough voltages, oxygen ions preferentially stored within the ZnO electrode diffuse back into the MLs due to electrical repulsion from the top electrode. As a consequence, oxygen vacancies will be filled and the CF partially reoxidizes next to the ZnO/MLs interface [Reset, Fig. 5(d)].<sup>42</sup> In this HRS and maintaining negative bias at the top electrode, electron-hole formation within the NCs takes place (as described above), which induces a clear Si NCs-related EL emission. After positive biasing, substrate inversion occurs, after which the injection of carriers into the MLs is reverted: only electrons are injected from the substrate [Fig. 5(e)]. Under the same conditions that applied for the pristine state, Si NC-related emission takes place. At this point, it is relevant to mention that, even when the electrical and EL properties of the pristine and HRS states should be equivalent, the former presents higher conductivity (see Fig. 2) and less intense EL under both applied polarities. This is due to the CFs being partially reoxidized after Reset, leaving some oxygen vacancies behind. Part of the injected current in the HRS is leaked through the remnants of the CF which contain non-confined Si NCs, and therefore a weaker EL intensity is expected from the rest of the unaltered Si NCs as only a part of the total current, and thus a lower current density, is circulating through them. A high applied positive polarity induces once more the movement of oxygen ions toward the top electrode. This process forms the CFs again and thus the device returns to the LRS [Set, Fig. 5(f)].

Finally, the hereby presented model, which is able to completely describe our observations, is in good agreement with most relevant reports on the topic. Some works have explored the behavior of Si oxides under resistive switching processes and their relation with Si NCs.<sup>11,30,50</sup> As well, the interaction of light in RS materials has also been explored, such as the case of light-activation of RS in the work of Mehonic *et al.*<sup>25</sup> and the reading of the RS state via optical absorption modulation in the work of Emboras *et al.*<sup>28</sup> Indeed, the occurrence of EL emission following (and thus being a consequence of) the RS cycle of a given dielectric material has been already reported only in few works, some of which include size-unconstrained matrix-embedded Si NCs.<sup>27,52</sup> Nevertheless, the

present work establishes a particular design, fabrication, and polarization method aiming at fully controlling and tuning the optical readout of the resistance state, making this unique combination of material and device structure a strong candidate for the next generation of light-integrating electronics.

## V. CONCLUSIONS

In summary, we have explored the RS and EL properties of Si NCs embedded into (*n*)ZnO/Si NC MLs/(*p*)Si device structures. It has been observed that the EL emitted at each resistance state (HRS and LRS) exhibits a distinguishable light emission after electrical excitation under both regimes (accumulation and inversion polarities). Of utter importance is not only the employed MIS design but also its particularities: whereas a Si<sub>3</sub>N<sub>4</sub> thin layer between substrate and the MLs enhances the electron injection probability from the substrate and thus electron-hole formation within the NCs, ZnO was employed as top transparent and EL-emitting electrode. The occurrence of additional light-emitting centers within the visible range (ZnO defects) to the well-known NIR Si NCs-related emission has demonstrated to allow for characteristic EL at each resistance state. In addition, the large difference in the EL emitted by the device structures under inversion electrical polarity for each resistance state allows for optically reading the resistance state of the device. As a consequence, the utilization of Si NCs within the present design could be the starting point for a new generation of EL memristors which can be exploited for the integration of photonics and electronics into the same physical location.

## ACKNOWLEDGMENTS

The authors thank Dr. L. López-Conesa and the group led by Professor F. Peiró for their help in the acquisition of the TEM images. This work was financially supported by the Spanish Ministry of Economy and Competitiveness (No. TEC2016-76849-C2-1-R) and the German Research Foundation (Nos. ZA191/27-3 and ZA191/33-1). J.V. is grateful for the funding through the Charles University center project (No. UNCE-SCI-010). J.L.F. acknowledges financial support from the subprogram “Ayudas para la Formación de Profesorado Universitario” (No. FPU16/06257) from the Spanish Ministry of Education, Culture and Sports for economical support. O.B. also acknowledges the subprogram “Ayudas para Contratos Predoctorales para la Formación de Doctores” from the Spanish Ministry of Economy and Competitiveness for economical support.

## REFERENCES

- <sup>1</sup>D. B. Strukov, G. S. Snider, D. R. Stewart, and R. S. Williams, “The missing memristor found,” *Nature* **453**(7191), 80–83 (2008).
- <sup>2</sup>I. Valov, “Redox-Based Resistive Switching Memories (ReRAMs): Electrochemical systems at the atomic scale,” *ChemElectroChem* **1**(1), 26–36 (2014).
- <sup>3</sup>D. S. Jeong, R. Thomas, R. S. Katiyar, J. F. Scott, H. Kohlstedt, A. Petraru, and C. S. Hwang, “Emerging memories: Resistive switching mechanisms and current status,” *Rep. Prog. Phys.* **75**(7), 076502 (2012).
- <sup>4</sup>I. Valov, R. Waser, J. R. Jameson, and M. N. Kozicki, “Electrochemical metallization memories—Fundamentals, applications, prospects,” *Nanotechnology* **22**(28), 289502 (2011).

- <sup>5</sup>R. Waser, R. Dittmann, C. Staikov, and K. Szot, "Redox-based resistive switching memories nanoionic mechanisms, prospects, and challenges," *Adv. Mater.* **21**(25–26), 2632–2663 (2009).
- <sup>6</sup>O. Blázquez, G. Martín, I. Camps, A. Mariscal, J. López-Vidrier, J. M. Ramírez, S. Hernández, S. Estradé, F. Peiró, R. Serna *et al.*, "Memristive behaviour of Si-Al oxynitride thin films: The role of oxygen and nitrogen vacancies in the electroforming process," *Nanotechnology* **29**(23), 235702 (2018).
- <sup>7</sup>G. Niu, P. Calka, M. A. der Maur, F. Santoni, S. Guha, M. Frascche, P. Hamoumou, B. Gautier, E. Perez, C. Walczyk *et al.*, "Geometric conductive filament confinement by nanotips for resistive switching of HfO<sub>2</sub>-RRAM devices with high performance," *Sci. Rep.* **6**(1), 25757 (2016).
- <sup>8</sup>K. M. Kim, S. Han, and C. S. Hwang, "Electronic bipolar resistance switching in an anti-serially connected Pt/TiO<sub>2</sub>/Pt structure for improved reliability," *Nanotechnology* **23**(3), 035201 (2012).
- <sup>9</sup>A. Mehonic, M. S. Munde, W. H. Ng, M. Buckwell, L. Montesi, M. Bosman, A. L. Shluger, and A. J. Kenyon, "Intrinsic resistance switching in amorphous silicon oxide for high performance SiO<sub>x</sub> ReRAM devices," *Microelectron. Eng.* **178**, 98–103 (2017).
- <sup>10</sup>M. S. Munde, A. Mehonic, W. H. Ng, M. Buckwell, L. Montesi, M. Bosman, A. L. Shluger, and A. J. Kenyon, "Intrinsic resistance switching in amorphous silicon suboxides: The role of columnar microstructure," *Sci. Rep.* **7**(1), 9274 (2017).
- <sup>11</sup>A. Mehonic, S. Cuffe, M. Wojdak, S. Hudziak, O. Jambois, C. Labbé, B. Garrido, R. Rizk, and A. J. Kenyon, "Resistive switching in silicon suboxide films," *J. Appl. Phys.* **111**(7), 074507 (2012).
- <sup>12</sup>F. Iacona, G. Franzò, and C. Spinella, "Correlation between luminescence and structural properties of Si nanocrystals," *J. Appl. Phys.* **87**(3), 1295–1303 (2000).
- <sup>13</sup>F. Iacona, G. Franzò, V. Vinciguerra, A. Irrera, and F. Priolo, "Influence of the spatial arrangement on the quantum confinement properties of Si nanocrystals," *Opt. Mater.* **17**(1–2), 51–55 (2001).
- <sup>14</sup>L. Khriachtchev, M. Räsänen, S. Novikov, and L. Pavesi, "Systematic correlation between Raman spectra, photoluminescence intensity, and absorption coefficient of silica layers containing Si nanocrystals," *Appl. Phys. Lett.* **85**(9), 1511–1513 (2004).
- <sup>15</sup>D. Kovalev, H. Heckler, G. Polisski, J. Diener, and F. Koch, "Optical properties of silicon nanocrystals," *Opt. Mater.* **17**(1–2), 35–40 (2001).
- <sup>16</sup>K. Kúsová, P. Hapala, J. Valenta, P. Jelínek, O. Cibulka, L. Ondič, and I. Pelant, "Direct bandgap silicon: Tensile-strained silicon nanocrystals," *Adv. Mater. Interf.* **1**(2), 1300042 (2014).
- <sup>17</sup>D. J. DiMaria, D. W. Dong, C. Falcony, T. N. Theis, J. R. Kirtley, J. C. Tsang, D. R. Young, F. L. Pesavento, and S. D. Brorson, "Charge transport and trapping phenomena in off-stoichiometric silicon dioxide films," *J. Appl. Phys.* **54**(10), 5801–5827 (1983).
- <sup>18</sup>I. Balberg, E. Savir, J. Jedrzejewski, A. G. Nassiopoulou, and S. Gardelis, "Fundamental transport processes in ensembles of silicon quantum dots," *Phys. Rev. B* **75**(23), 235329 (2007).
- <sup>19</sup>I. Balberg, "Electrical transport mechanisms in three dimensional ensembles of silicon quantum dots," *J. Appl. Phys.* **110**(6), 061301 (2011).
- <sup>20</sup>G. Franzò, A. Irrera, E. C. Moreira, M. Miritello, F. Iacona, D. Sanfilippo, G. Di Stefano, P. G. Fallica, and F. Priolo, "Electroluminescence of silicon nanocrystals in MOS structures," *Appl. Phys. A* **74**(1), 1–5 (2002).
- <sup>21</sup>A. Irrera, D. Pacifici, M. Miritello, G. Franzò, F. Priolo, F. Iacona, D. Sanfilippo, G. Di Stefano, and P. G. Fallica, "Electroluminescence properties of light emitting devices based on silicon nanocrystals," *Physica E* **16**(3–4), 395–399 (2003).
- <sup>22</sup>A. Fojtik, J. Valenta, T. H. Stuchlíková, J. Stuchlík, I. Pelant, and J. Kočka, "Electroluminescence of silicon nanocrystals in p–i–n diode structures," *Thin Solid Films* **515**(2), 775–777 (2006).
- <sup>23</sup>M. Zacharias and P. Streitenberger, "Crystallization of amorphous superlattices in the limit of ultrathin films with oxide interfaces," *Phys. Rev. B* **62**(12), 8391–8396 (2000).
- <sup>24</sup>M. Zacharias, J. Heitmann, R. Scholz, U. Kahler, M. Schmidt, and J. Bläsing, "Size-controlled highly luminescent silicon nanocrystals: A SiO/SiO<sub>2</sub> superlattice approach," *Appl. Phys. Lett.* **80**(4), 661–663 (2002).
- <sup>25</sup>A. Mehonic, T. Gerard, and A. J. Kenyon, "Light-activated resistance switching in SiO<sub>x</sub> RRAM devices," *Appl. Phys. Lett.* **111**(23), 233502 (2017).
- <sup>26</sup>C. Hoessbacher, Y. Fedoryshyn, A. Emboras, A. Melikyan, M. Kohl, D. Hillerkuss, C. Hafner, and J. Leuthold, "The plasmonic memristor: A latching optical switch," *Optica* **1**(4), 198 (2014).
- <sup>27</sup>A. A. Zakhidov, B. Jung, J. D. Slinker, H. D. Abruña, and G. G. Malliaras, "A light-emitting memristor," *Org. Electron.* **11**(1), 150–153 (2010).
- <sup>28</sup>A. Emboras, I. Goykhman, B. Desiatov, N. Mazurski, L. Stern, J. Shappir, and U. Levy, "Nanoscale plasmonic memristor with optical readout functionality," *Nano Lett.* **13**(12), 6151–6155 (2013).
- <sup>29</sup>U. Koch, C. Hoessbacher, A. Emboras, and J. Leuthold, "Optical memristive switches," *J. Electroceramics* **39**(1–4), 239–250 (2017).
- <sup>30</sup>K. E. González-Flores, B. Palacios-Márquez, J. Álvarez-Quintana, S. A. Pérez-García, L. Licea-Jiménez, P. Horley, and A. Morales-Sánchez, "Resistive switching control for conductive Si-nanocrystals embedded in Si/SiO<sub>2</sub> multilayers," *Nanotechnology* **29**(39), 395203 (2018).
- <sup>31</sup>A. Marconi, A. Anopchenko, M. Wang, G. Pucker, P. Bellutti, and L. Pavesi, "High power efficiency in Si-Nc/SiO<sub>2</sub> multilayer light emitting devices by bipolar direct tunneling," *Appl. Phys. Lett.* **94**(22), 221110 (2009).
- <sup>32</sup>A. Anopchenko, A. Marconi, E. Moser, S. Prezioso, M. Wang, L. Pavesi, G. Pucker, and P. Bellutti, "Low-voltage onset of electroluminescence in nanocrystalline-Si/SiO<sub>2</sub> multilayers," *J. Appl. Phys.* **106**(3), 033104 (2009).
- <sup>33</sup>J. López-Vidrier, Y. Berencén, S. Hernández, O. Blázquez, S. Gutsch, J. Laube, D. Hiller, P. Löper, M. Schnabel, S. Janz *et al.*, "Charge transport and electroluminescence of silicon nanocrystals/SiO<sub>2</sub> superlattices," *J. Appl. Phys.* **114**(16), 163701 (2013).
- <sup>34</sup>J. López-Vidrier, Y. Berencén, S. Hernández, B. Mundet, S. Gutsch, J. Laube, D. Hiller, P. Löper, M. Schnabel, S. Janz *et al.*, "Structural parameters effect on the electrical and electroluminescence properties of silicon nanocrystals/SiO<sub>2</sub> superlattices," *Nanotechnology* **26**(18), 185704 (2015).
- <sup>35</sup>J. López-Vidrier, S. Gutsch, O. Blázquez, J. Valenta, D. Hiller, J. Laube, J. Blanco-Portals, L. López-Conesa, S. Estradé, F. Peiró *et al.*, "Effect of Si<sub>3</sub>N<sub>4</sub>-mediated inversion layer on the electroluminescence properties of silicon nanocrystal superlattices," *Adv. Electron. Mater.* **4**, 1700666 (2018).
- <sup>36</sup>Y. Berencén, J. M. Ramírez, O. Jambois, C. Domínguez, J. A. Rodríguez, and B. Garrido, "Correlation between charge transport and electroluminescence properties of Si-rich oxide/nitride/oxide-based light emitting capacitors," *J. Appl. Phys.* **112**(3), 033114 (2012).
- <sup>37</sup>A. M. Hartel, D. Hiller, S. Gutsch, P. Löper, S. Estradé, F. Peiró, B. Garrido, and M. Zacharias, "Formation of size-controlled silicon nanocrystals in plasma enhanced chemical vapor deposition grown SiO<sub>x</sub>N<sub>y</sub>/SiO<sub>2</sub> superlattices," *Thin Solid Films* **520**(1), 121–125 (2011).
- <sup>38</sup>S. Gutsch, D. Hiller, J. Laube, M. Zacharias, and C. Kübel, "Observing the morphology of single-layered embedded silicon nanocrystals by using temperature-stable TEM membranes," *Beilstein J. Nanotechnol.* **6**(1), 964–970 (2015).
- <sup>39</sup>J. Laube, S. Gutsch, D. Wang, C. Kübel, M. Zacharias, and D. Hiller, "Two-dimensional percolation threshold in confined Si nanoparticle networks," *Appl. Phys. Lett.* **108**(4), 043106 (2016).
- <sup>40</sup>J. Laube, D. Nübling, H. Beh, S. Gutsch, D. Hiller, and M. Zacharias, "Resistivity of atomic layer deposition grown ZnO: The influence of deposition temperature and post-annealing," *Thin Solid Films* **603**, 377–381 (2016).
- <sup>41</sup>H. Beh, D. Hiller, J. Laube, S. Gutsch, and M. Zacharias, "Deposition temperature dependence and long-term stability of the conductivity of undoped ZnO grown by atomic layer deposition," *J. Vac. Sci. Technol. A* **35**(1), 01B127 (2017).
- <sup>42</sup>O. Blázquez, J. L. Frieiro, J. López-Vidrier, C. Guillaume, X. Portier, C. Labbé, P. Sanchis, S. Hernández, and B. Garrido, "Resistive switching and charge transport mechanisms in ITO/ZnO/p-Si devices," *Appl. Phys. Lett.* **113**(18), 183502 (2018).
- <sup>43</sup>J. López-Vidrier, S. Gutsch, O. Blázquez, D. Hiller, J. Laube, R. Kaur, S. Hernández, B. Garrido, and M. Zacharias, "Modulation of the electroluminescence emission from ZnO/Si NCs/p-Si light-emitting devices via pulsed excitation," *Appl. Phys. Lett.* **110**(20), 203104 (2017).

- <sup>44</sup>J. López-Vidrier, S. Hernández, D. Hiller, S. Gutsch, L. López-Conesa, S. Estradé, F. Peiró, M. Zacharias, and B. Garrido, "Annealing temperature and barrier thickness effect on the structural and optical properties of silicon nanocrystals/SiO<sub>2</sub> superlattices," *J. Appl. Phys.* **116**(13), 133505 (2014).
- <sup>45</sup>J. López-Vidrier, S. Hernández, A. M. Hartel, D. Hiller, S. Gutsch, P. Löper, L. López-Conesa, S. Estradé, F. Peiró, M. Zacharias *et al.*, "Structural and optical characterization of size controlled silicon nanocrystals in SiO<sub>2</sub>/SiO<sub>x</sub>N<sub>y</sub> multilayers," *Energy Procedia* **10**, 43–48 (2011).
- <sup>46</sup>Y. Chen, D. M. Bagnall, H. Koh, K. Park, K. Hiraga, Z. Zhu, and T. Yao, "Plasma assisted molecular beam epitaxy of ZnO on c-plane sapphire: Growth and characterization," *J. Appl. Phys.* **84**(7), 3912–3918 (1998).
- <sup>47</sup>S. Gutsch, J. Laube, A. M. Hartel, D. Hiller, N. Zakharov, P. Werner, and M. Zacharias, "Charge transport in Si nanocrystal/SiO<sub>2</sub> superlattices," *J. Appl. Phys.* **113**(13), 133703 (2013).
- <sup>48</sup>D. Hiller, A. Zelenina, S. Gutsch, S. A. Dyakov, L. López-Conesa, J. López-Vidrier, S. Estradé, F. Peiró, B. Garrido, J. Valenta *et al.*, "Absence of quantum confinement effects in the photoluminescence of Si<sub>3</sub>N<sub>4</sub>-embedded Si nanocrystals," *J. Appl. Phys.* **115**(20), 204301 (2014).
- <sup>49</sup>A. X. Chu and W. B. Fowler, "Theory of oxide defects near the Si-SiO<sub>2</sub> interface," *Phys. Rev. B* **41**(8), 5061–5066 (1990).
- <sup>50</sup>J. Yao, L. Zhong, D. Natelson, and J. M. Tour, "In situ imaging of the conducting filament in a silicon oxide resistive switch," *Sci. Rep.* **2**(1), 242 (2012).
- <sup>51</sup>A. Zimina, S. Eisebitt, W. Eberhardt, J. Heitmann, and M. Zacharias, "Electronic structure and chemical environment of silicon nanoclusters embedded in a silicon dioxide matrix," *Appl. Phys. Lett.* **88**(16), 163103 (2006).
- <sup>52</sup>C. He, J. Li, X. Wu, P. Chen, J. Zhao, K. Yin, M. Cheng, W. Yang, G. Xie, D. Wang *et al.*, "Tunable electroluminescence in planar graphene/SiO<sub>2</sub> memristors," *Adv. Mater.* **25**(39), 5593–5598 (2013).